

DESIGN OF A NOVEL BROADBAND EMC DOUBLE RIDGED GUIDE HORN ANTENNA

Tenigeer*, Ning Zhang, Jinghui Qiu, Pengyu Zhang, and Yang Zhang

School of Electronics and Information Engineering, Harbin Institute of Technology, Heilongjiang 150080, China

Abstract—An improved double ridged horn antenna (DRHA) is proposed in this paper. By adding the dielectric lens at the aperture of the horn, radiation pattern distortion arising in the high frequency band of conventional DRHA is improved, which leads to higher radiation gain. Meanwhile, ridge slot loading contributes to better impedance matching characteristic, broadening the impedance bandwidth efficiently. The improved antenna is fabricated and measured, with the measured results consist with the simulation perfectly, which proved the viability of the improvement.

1. INTRODUCTION

Horn antennas are widely used in various fields, such as Electromagnetic Compatibility (EMC) testing, standard gain testing, satellite tracking systems, launching feeds, radars, etc. [1–3]. The reason for choosing horn antennas in these applications is based on its unique characteristics: easy feeding, relatively simple construction, high gain and excellent peak power handling capability [4–8]. However, due to the development of wideband testing systems, applications of conventional horn antennas become more and more limited. Acting like band-pass filters, horn antennas have limited bandwidth, so methods for broadening antennas' widest working frequency band are in urgent need. Ridged waveguides came to use in the 1960s [9, 10]. Capacitive effects caused by ridges in waveguides or horns help lower the cutoff frequency of the dominant mode (TE_{10}) and broaden the single-mode bandwidth. Radiation pattern distortion arises in the high frequency band in conventional ridged horn antennas, caused by greater phase

Received 28 March 2013, Accepted 26 April 2013, Scheduled 8 May 2013

* Corresponding author: Tenigeer (tnge1983@sina.com).

error at the antenna aperture when the frequency gets higher. To overcome the problem, according to [10–13] dielectric lens loading is introduced in this paper to reduce the phase error at the aperture, which helps improve antennas' radiation patterns in the high frequency band and increase radiation gain in the whole frequency band; meanwhile, a novel ridge structure with slot loading on ridges is adopted in this paper and the simulated and measured results show that the impedance matching characteristic of the antenna in the lower frequency band is improved greatly due to the addition of the slot loading.

DRGH design is divided into 4 parts: characteristic impedance calculation of ridged waveguides by transverse resonant method combined with the calculation method in [14–16], the design of the reflection cavity design of the ridged structure extending from the waveguide port to the horn aperture and structure optimization which includes analysis of phase error distribution at the antenna aperture, design of dielectric lens according to the structure, analysis of ridged waveguide and design of slot loading on ridges for lowering the cutoff frequency of the dominant mode (TE_{10}). Fig. 1 shows the conventional ridged horn antenna structure.

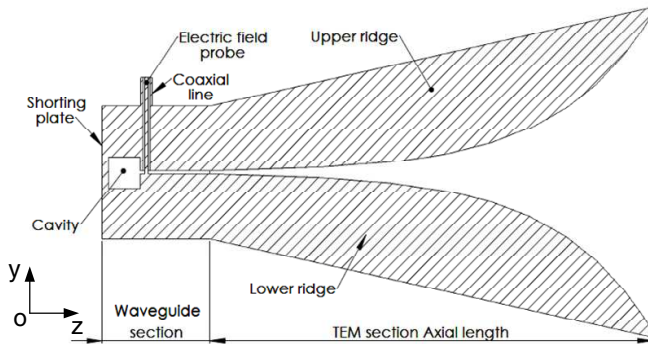


Figure 1. Side view of the antenna model.

2. ANTENNA GEOMETRY AND DESIGN

2.1. Feeding Ridged Waveguide Analysis

Double ridges in the rectangular waveguides can be approximated as capacitive susceptances according to transverse resonant method. Fig. 2 shows the cross sectional view of a ridged waveguide and equivalent lumped-constant circuit of a ridged waveguide.

According to formulas (1) and (2) adopted from [14], the plate capacitance per unit length of RWG (ridged waveguide) convex part

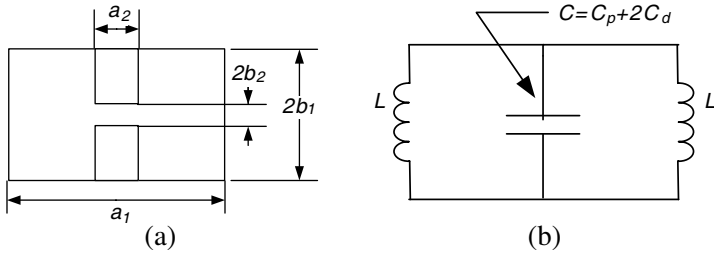


Figure 2. Waveguide section of the DRGH. (a) Cross sectional view of a ridged waveguide. (b) Equivalent lumped-constant circuit for a ridged waveguide.

and discontinuity capacitance per unit length C_d can be calculated. The total capacitance per unit length of the ridged waveguide C (F/m) is obtained as follow:

$$C = C_p + 2C_d \tag{1}$$

The total inductance per unit length L (H/m):

$$L = \frac{1}{2} \frac{\mu (a_1 - a_2) b_1}{2} \tag{2}$$

When λ_c refers to the cutoff wavelength of the dominant mode (TE₁₀) in rectangular waveguides, i.e., $\lambda_c = 2a_1$, the cutoff wavelength ratio in waveguides with and without ridges is:

$$\frac{\lambda'_c}{\lambda_c} = \frac{\pi}{2} \sqrt{\left(\frac{a_2}{b_2} + \frac{2C_d}{\epsilon}\right) \left(\frac{b_1}{a_1}\right) \left(1 - \frac{a_2}{a_1}\right)} \tag{3}$$

According to formula (6) in [14], the cutoff frequency of rectangular ridged waveguides is:

$$f'_c = \frac{1}{2\pi\sqrt{LC}} = \frac{1}{\pi\sqrt{\mu\epsilon}\sqrt{\left(\frac{a_2}{b_2} + \frac{2C_d}{\epsilon}\right) (a_1 - a_2) b_1}} \tag{4}$$

The characteristic impedance of the dominant mode (TE₁₀) can be calculated as follow when the frequency is infinite:

$$Z_{0\infty} = \frac{120\pi}{\frac{2C_d}{\epsilon} \cos\left(\frac{a_2 \lambda_c \pi}{a_1 \lambda'_c 2}\right) + \frac{1}{\pi} \frac{\lambda'_c}{b_2} \left(\sin\left(\frac{a_2 \lambda_c \pi}{a_1 \lambda'_c 2}\right) + \frac{b_2}{b_1} \cos\left(\frac{a_2 \lambda_c \pi}{a_1 \lambda'_c 2}\right) \tan\left(\left(1 - \frac{a_2}{a_1}\right) \frac{\lambda_c \pi}{\lambda'_c 2}\right) / 2\right)} \tag{5}$$

Characteristic impedance corresponding to finite frequency f can be calculated as:

$$Z_0 = Z_{0\infty} / \sqrt{1 - (f'_c/f)^2} \tag{6}$$

λ'_c/λ_c of the dominant mode can be calculated according to the known values of b_1/a_1 , b_2/b_1 , a_2/a_1 and formula (3). Then the characteristic impedance of ridged waveguides at infinite frequency can be calculated according to formula (5). The corresponding dimensions of the ridged waveguide are: $a_1 = 27$ mm, $2b_1 = 19$ mm, $a_2 = 3.5$ mm, $2b_2 = 0.5$ mm. The cutoff wavelength and characteristic impedance changing curves with frequency is plotted in Fig. 3, where $b_1/a_1 = 0.35$. So we can get that $f_c = 1.58$ GHz and $Z_{0\infty} = 43 \Omega$ according to formula (1)–(6).

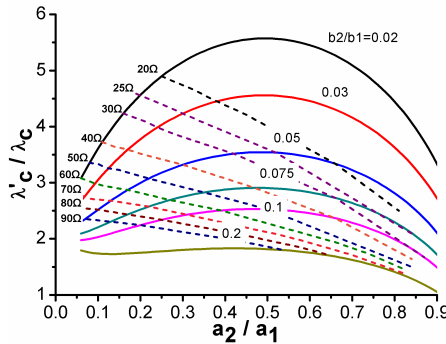


Figure 3. Characteristic impedance and cutoff wavelength of ridge wave guide ($b_1/a_1 = 0.35$).

2.2. Design of Cavity Section

Figure 4 shows the configuration of the reflection cavity. After simulating models with different h and d , the optimized structure dimensions are achieved. As shown in Fig. 5, the optimized impedance matching is achieved when d equals to 10 mm and h equals to 2 mm. On the condition that S_{11} is less than -7.5 dB, the working frequency band ranges from 2 GHz to 40 GHz.

2.3. Design of the Ridge Loaded Flared Section

The aperture dimension of the horn is 50 mm \times 50 mm, and the TEM section axial length $L = 70$ mm. The changing height of the ridges is consistent with the changing characteristic impedance from the

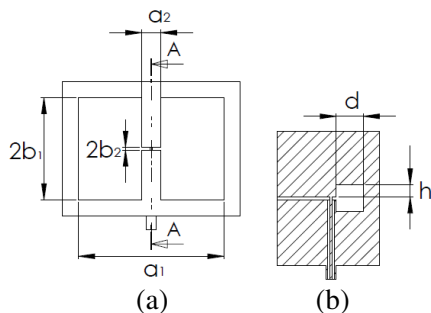


Figure 4. The structure of the reflection cavity. (a) Front view. (b) Sectional view

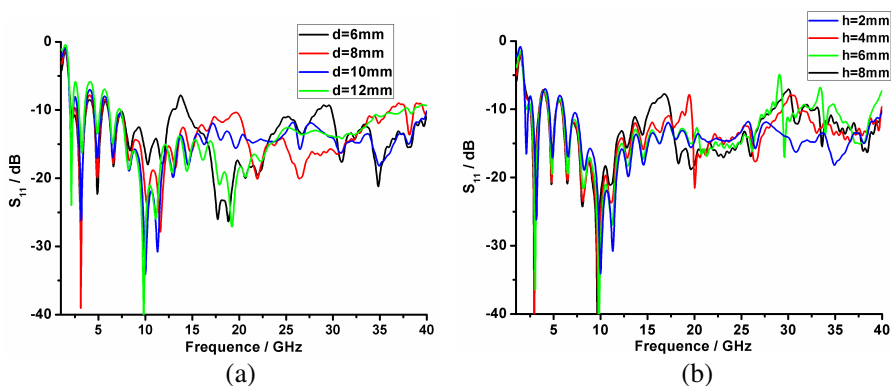


Figure 5. Return loss plotted versus frequency with different d and h .

rectangular ridged waveguide to the free space (377Ω). The changing curve of the ridge is given in formula (7) and (8).

$$y(z) = \frac{s}{2} \times \exp^{\beta z} \quad (0 \leq z \leq L) \tag{7}$$

with

$$\beta = \frac{1}{L} \ln \left(\frac{y_{ap}}{s} \right) \tag{8}$$

where the horn aperture distance $y_{ap} = 50 \text{ mm}$ and the gap between the ridges in the feeding waveguide s is equal to 0.5 mm .

To improve the antenna's impedance characteristic in the lower frequency band further, slot loading on the ridges is adopted which can change the current distribution on the ridges leading to different

equivalent capacitance. Fig. 6 shows the structure of slot loading where $L = 70$ mm, $L1 = 57$ mm, $L2 = 16$ mm, $W = 50$ mm, $W1 = 1.5$ mm, $W2 = 15.3$ mm, $y_{ap} = 50$ mm. The influence of the position of the starting point on S_{11} is shown in Fig. 7. Fig. 8 shows S_{11} comparison between antennas with and without slot loading. The novel antenna improves the impedance matching greatly in the frequency band of 2 GHz–7 GHz. The working frequency band ranges from 2 GHz to 40 GHz when S_{11} is less than -10 dB.

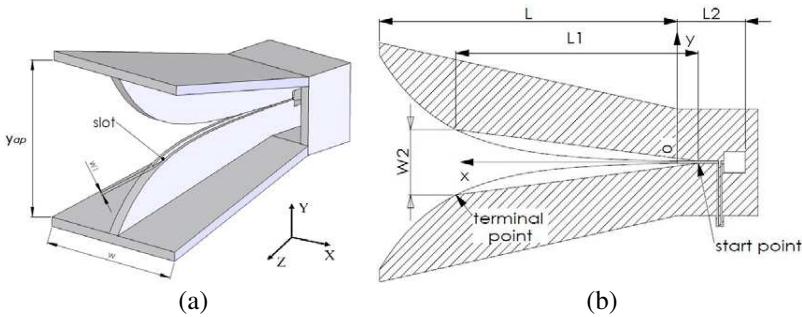


Figure 6. Slot loading ridged horn. (a) Antenna phototype. (b) Cross-section drawn.

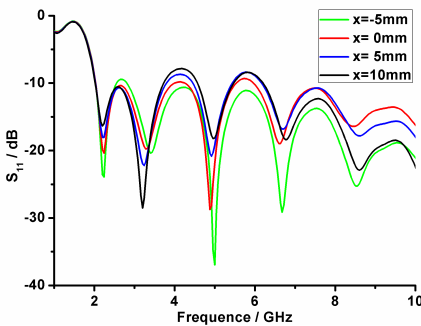


Figure 7. Simulated S_{11} versus frequency for various starting points.

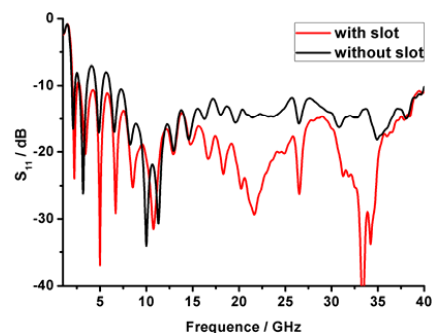


Figure 8. Comparison of S_{11} versus.

2.4. The Design of the Lens

According to the analysis in [17], single-face lens can be utilized to decrease the phase error at the aperture regarding the antenna

proposed in this paper and increase the radiation gain. According to Fermat principle which states that the phase error can be decreased when the traveling distances of light from the feed to the aperture are equivalent in all directions, the lens curve can be calculated as follow:

$$y = \sqrt{(n^2 - 1)z^2 + 2(n - 1)(L - d)z} \quad (0 \leq z \leq d) \quad (9)$$

where n refers to the reflection coefficient of the lens, and $n = \sqrt{\epsilon_r}$. Teflon with the dielectric constant of 2.2 ($\tan \delta = 0.0002$) is used in this antenna. d refers to the maximal thickness of the lens, which equals to 8.7 mm here. Fig. 9 shows the double-ridged horn antenna loaded with lens.

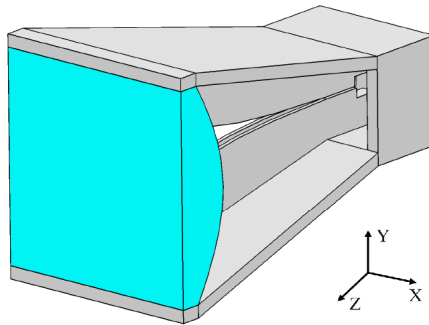


Figure 9. Double-ridged horn antenna loaded with lens.

3. SIMULATION AND MEASUREMENT RESULTS

Voltage Standing Wave Ratio (VSWR), radiation patterns and gain of the designed antenna are simulated by CST MICROWAVE STUDIO in this chapter; then the antenna is fabricated and measured. Fig. 10 shows the prototype of the antenna fabricated which is to be measured then. The measured results coincide with the simulation well, which proved the rationality of the design.

Figure 11 shows that VSWR of the antenna is less 2 from 2 GHz to 40 GHz, which indicates that the measurement coincides with the simulation well except for the small difference in the high frequency band caused by fabrication error and the effect from SMA connector when the frequency is high.

Figure 12 shown that the phase error between the aperture center and the edges decreases greatly, leading to more uniform phase distribution, which lowers the sidelobe level of the radiation pattern and enhance the gain.

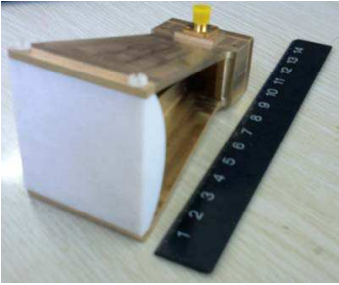


Figure 10. Antenna prototype.

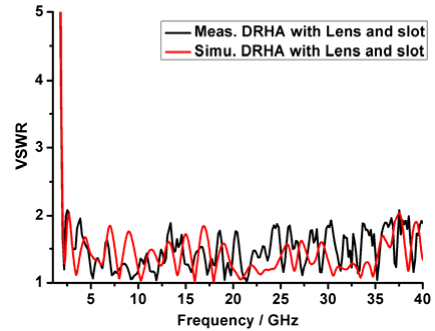


Figure 11. Simulated and measured VSWR of the antenna.

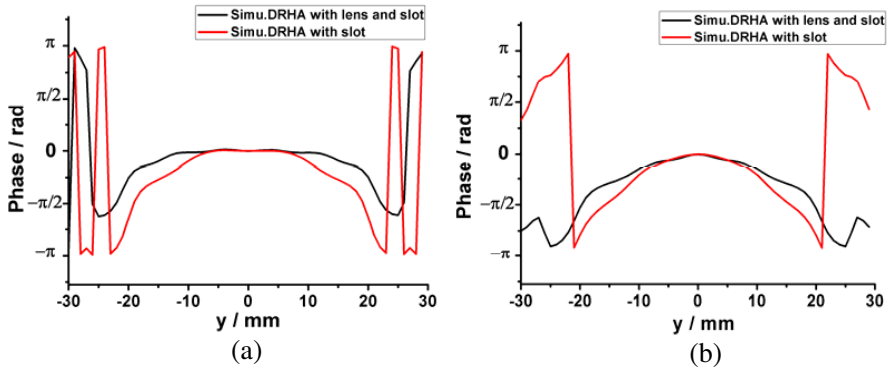


Figure 12. Electrical field phase distribution along y -axis. (a) 25 GHz. (b) 28 GHz.

Simulated and measured results of antenna gain are shown in Fig. 13, where the red curve indicates the gain of DRHA without dielectric lens loading. The gain in the main direction decreases in the frequency band of 25 GHz–30 GHz obviously, which is caused by radiation pattern distortion due to great phase error across the aperture of the antenna when the frequency gets higher. Dielectric lens loading can help decrease the error and enhance the gain.

It shows that gain decreases greatly at 28 GHz without lens loading in Fig. 13. 3D radiation pattern comparison between antennas with and without lens loading at the frequency of 28 GHz is shown in Fig. 14. Serious radiation pattern distortion arises in the antenna without the dielectric lens loading, leading to decreased gain in the main radiation direction; dielectric lens loading contributes greatly to stable radiation

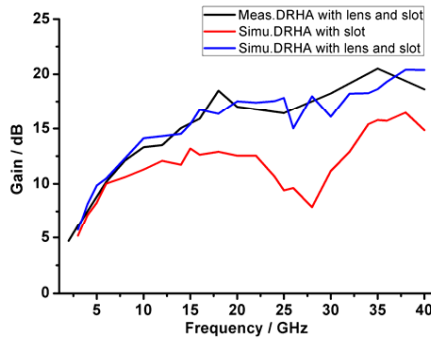


Figure 13. Simulated and measured results of antenna gain.

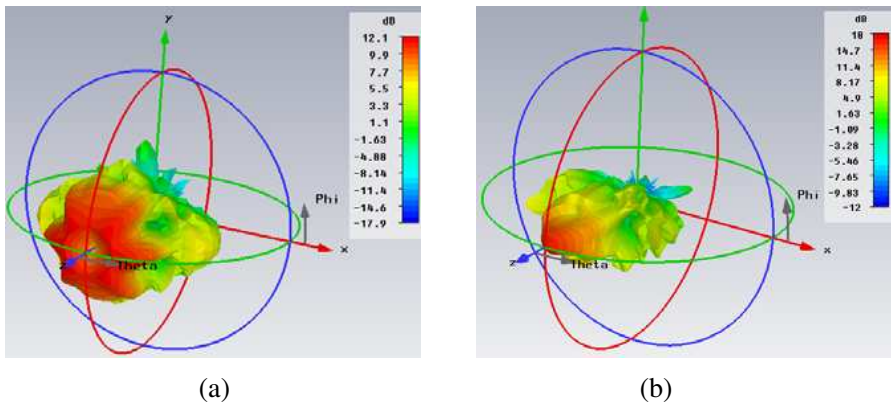
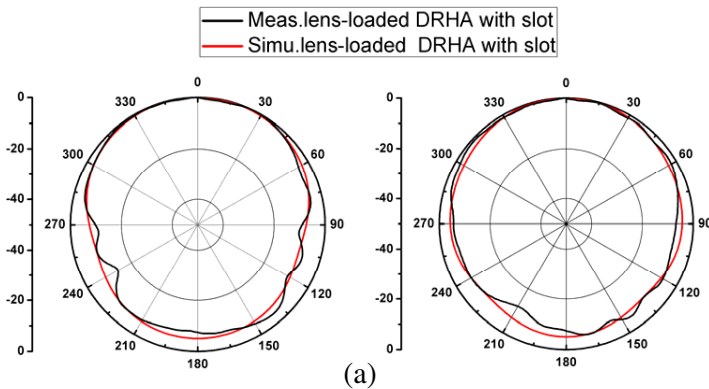


Figure 14. Radiation patterns at 20 GHz. (a) Without lens loading. (b) Loaded with lens.



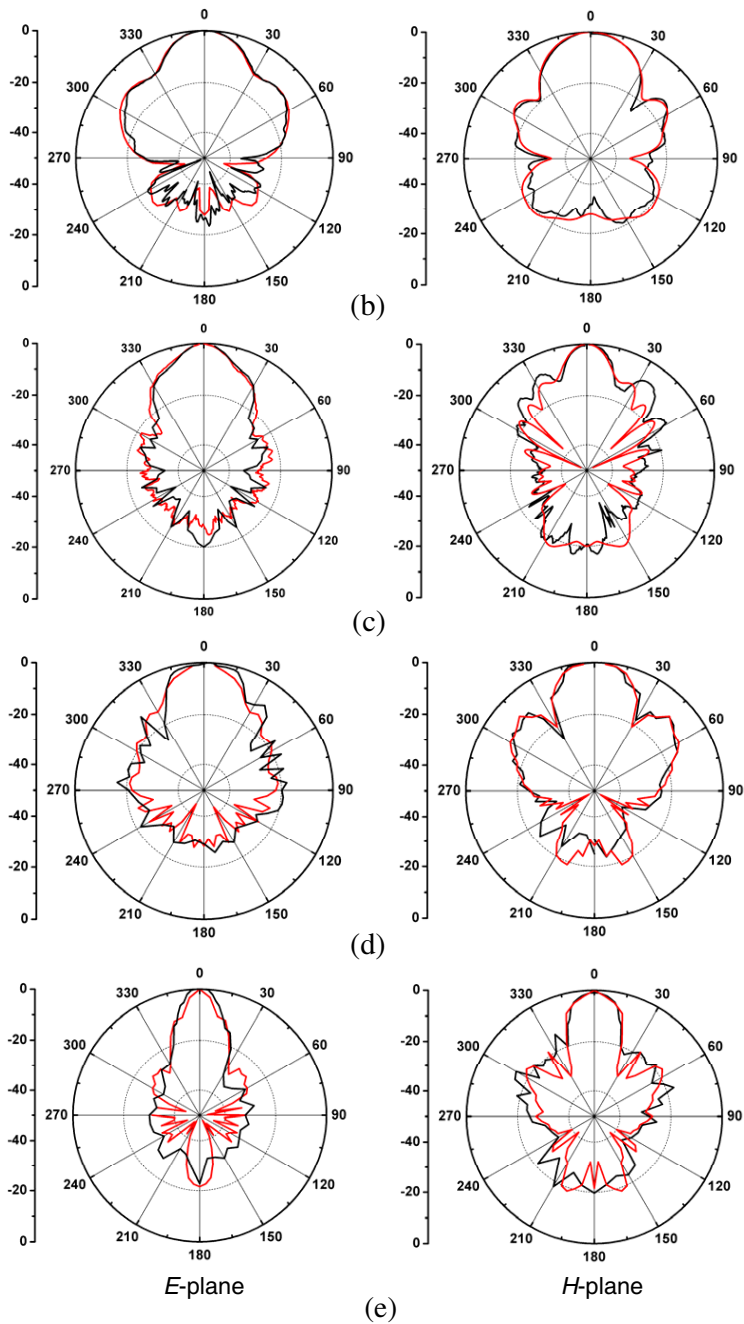


Figure 15. *E*-plane and *H*-plane radiations pattern of the antennas at (a) 2 GHz, (b) 10 GHz, (c) 20 GHz, (d) 30 GHz, (e) 40 GHz.

patterns along with higher gain, which proves the rationality of the design further.

Simulated and measured E -plane and H -plane radiation patterns of the ridged antenna with dielectric lens and slot loading are shown in Fig. 15, at the frequencies of 2 GHz, 10 GHz, 20 GHz, 30 GHz and 40 GHz respectively. It's shown that the simulation coincides with the measurement well, where 3 dB beamwidths are 15° – 100° and 10° – 80° in the H plane and E plane respectively.

4. CONCLUSION

A novel ridged horn ultra-wideband antenna is proposed in this paper. Impedance and radiation characteristics are improved greatly by introducing dielectric lens and slots on the ridges compared to conventional ridged horn antennas. The designed antenna is fabricated and measured, with the measured results consist with the simulation well. The working bandwidth of the antenna is from 2 GHz to 40 GHz when VSWR is less than 2. Gain changes from 5 dB to 20 dB in the whole frequency band, which proves the rationality of the theoretical analysis and simulation.

REFERENCES

1. Abbas-Azimi, M., F. Arazm, and J. Rashed-Mohassel, "Design of a new broadband EMC double ridged guide horn antenna," *First European Conference on Antennas and Propagation, EuCAP*, 1–5, 2006.
2. Ghorbani, M. A. and A. Khaleghi, "Double ridged horn antenna designs for wideband applications," *2011 19th Iranian Conference on Electrical Engineering (ICEE)*, 1–4, 2011.
3. Jacobs, B., J. W. Odendaal, and J. Joubert, "An improved design for a 1–18 GHz double-ridged guide horn antenna," *IEEE Transactions on Antennas and Propagation*, Vol. 60, No. 9, 4110–4118, 2012.
4. Dehdasht-Heydari, R., H. R. Hassani, and A. R. Mallahzadeh, "A new 2–18 GHz quad-ridged horn antenna," *Progress In Electromagnetics Research*, Vol. 81, 183–195, 2008.
5. Dehdasht-Heydari, R., H. R. Hassani, and A. R. Mallahzadeh, "Quad ridged horn antenna for UWB applications," *Progress In Electromagnetics Research*, Vol. 79, 23–38, 2008.
6. Mallahzadeh, A. R., A. A. Dastranj, and H. R. Hassani, "A novel dual-polarized double-ridged horn antenna for wideband

- applications,” *Progress In Electromagnetics Research B*, Vol. 1, 67–80, 2008.
7. Liu, J., Y. Zhou, and J. Zhu, “Research and design of quadruple-ridged horn antenna,” *Progress In Electromagnetics Research Letters*, Vol. 37, 21–28, 2013.
 8. Abbas-Azimi, M., F. Arazm, and J. Rashed-Mohassel, “Sensitivity analysis of a 1 to 18 GHz broadband DRGH antenna,” *IEEE Antennas and Propagation Society International Symposium*, 3129–3132, 2006.
 9. Botello-Perez, M., H. Jardon-Aguilar, and I. G. Ruiz, “Design and simulation of a 1 to 14 GHz broadband electromagnetic compatibility DRGH antenna,” *2005 2nd International Conference on Electrical and Electronics Engineering*, 118–121, 2005.
 10. Lai, H., R. Franks, D. Kong, D. Kuck, and T. Gackstetter, “A broad band high efficient quad ridged horn,” *IEEE Antennas and Propagation Society International Symposium*, Vol. 25, 676–679, 1987.
 11. Qiu, J. H., Y. Suo, and W. Li, “Research and design on ultra-wideband dielectric hemispheric lens loaded quad-ridged horn antenna,” *2007 6th International Conference on Antenna Theory and Techniques*, 253–255, 2007.
 12. Bauerle, R. J., R. Schrimpf, E. Gyorko, and J. Henderson, “The use of a dielectric lens to improve the efficiency of a dual-polarized quad-ridge horn from 5 to 15 GHz,” *IEEE Transactions on Antennas and Propagation*, Vol. 57, 1822–1825, 2009.
 13. Serdar, T. and K. A. Kenan, “Partially dielectric-loaded ridged horn antenna design for ultrawideband gain and radiation performance enhancement,” *IEEE Antennas and Wireless Propagation Letters*, Vol. 11, 921–924, 2012.
 14. Chen, T.-S., “Calculation of the parameters of ridge waveguides,” *IRE Transactions on Microwave Theory and Techniques*, Vol. 5, No. 1, 12–17, 1957.
 15. Cohn, S. B., “Properties of ridge wave guide,” *Proceedings of the IRE*, Vol. 35, No. 8, 783–788, 1947.
 16. Hopfer, S., “The design of ridged waveguides,” *IRE Transactions on Microwave Theory and Techniques*, Vol. 3, No. 5, 20–29, 1955.
 17. Milligan, T. A., *Modern Antenna Design*, 2nd Edition, 448–451, Hoboken, New Jersey, USA, 2005.